2006-08-21

Recovering Grain Boundary Inclination Parameters Through Oblique Double-Sectioning

Eric Richards Homer
Brigham Young University - Provo

RECOVERING GRAIN BOUNDARY INCLINATION PARAMETERS THROUGH OBLIQUE DOUBLE-SECTIONING

by

Eric Richards Homer

A thesis submitted to the faculty of

Brigham Young University

in partial fulfillment of the requirements for the degree of

Master of Science

Department of Mechanical Engineering

Brigham Young University

December 2006

BRIGHAM YOUNG UNIVERSITY

GRADUATE COMMITTEE APPROVAL

of a thesis submitted by

Eric Richards Homer

This thesis has been read by each member of the following graduate committee and by majority vote has been found to be satisfactory.

Date	Brent L. Adams, Chair
Date	Michael P. Miles
Date	Brian D. Jensen

BRIGHAM YOUNG UNIVERSITY

As chair of the candidate's graduate committee, I have read the thesis of Eric Richards Homer in its final form and have found that (1) its format, citations, and bibliographical style are consistent and acceptable and fulfill university and department style requirements; (2) its illustrative materials including figures, tables, and charts are in place; and (3) the final manuscript is satisfactory to the graduate committee and is ready for submission to the university library.

Date

Brent L. Adams
Chair, Graduate Committee

Accepted for the Department

Mathew R. Jones
Graduate Coordinator

Accepted for the College

Alan R. Parkinson
Dean, Ira A. Fulton College of Engineering and Technology

ABSTRACT

RECOVERING GRAIN BOUNDARY INCLINATION PARAMETERS THROUGH OBLIQUE DOUBLE-SECTIONING

Eric Richards Homer

Department of Mechanical Engineering

Master of Science

A method for the retrieval of grain boundary inclination parameters of the grain boundary character distribution by oblique double-sectioning is proposed. The method, which is similar to the recovery of the orientation distributions from sets of incomplete pole-figures, is described along with a framework for implementation.

The method directly measures grain boundary inclinations in a manner similar to serial sectioning while statistically sampling the microstructure comparably to stereological methods.

Computer simulations of the method were used to confirm the mathematical framework. Additional simulations, where the grain boundary normal distributions were recovered by both oblique double-sectioning and stereological methods, showed that results recovered by 3 orthogonal double-sections from oblique double-sectioning

proved to be just as accurate as the 25 section-cuts required for stereology in resolving the finer details in the recovered distribution.

ACKNOWLEDGMENTS

I would like to thank my advisor, Dr Brent Adams for his help and guidance throughout the past few years of research. He has been an excellent mentor and provided me with so many opportunities from which I have been able to learn and grow. I would also like to thank those in the Microstructure Sensitive Design research group for their support and contributions. It has been a pleasure to work with each of the members of the group.

I would especially like to thank Sarah, my wife, for her unending support and love. This project would not have been completed without her support. Finally, I would like to thank my Heavenly Father, without whose blessings I could not have completed this thesis.

TABLE OF CONTENTS

LIST OF TABLES

LIST OF FIGURES

1 Background

1.1 Motivation

Polycrystalline materials are by nature largely affected by their internal interfaces. In fact, it has been said that the study of polycrystalline materials can be reduced to the study of their interfaces [1]. As our understanding of the grain boundary character has increased, so has our ability to improve materials properties. Grain boundary engineering (GBE) has recently emerged as a promising way to improve macroscopic material properties by controlling the grain boundary character of a material [2]. For example, both Watanabe et al. and Schwartz et al. show how specialized processing routes in the presence of magnetic fields or specific thermomechanical processing can be used to manipulate the grain boundary character for improved performance [3,4].

Essential to all these improvements is, of course, our ability to properly characterize the material behavior. A common representation that has been introduced for this purpose is the grain boundary character distribution (GBCD). The work presented herein is aimed at describing a new and efficient technique through which one can obtain the GBCD of a material.

While the GBCD can be largely affected by the grain boundary plane orientation, quite often the GBCD has been defined solely in terms of the crystallographic misorientation across the grain boundaries in a material. This is due in large part to the challenge associated with recovering the boundary inclination in polycrystalline materials. In addition to this challenge, misorientation characteristics, efficiently captured in the sigma number associated with coincident site lattice (CSL) theory, have correlated well with grain boundary properties such as improved resistance to stress corrosion cracking (SCC). Although these recognition schemes do not always work, several studies have illustrated that the CSL boundaries, determined by grain boundary misorientation, have often exhibited an increased resistance to different modes of failure [5-8].

For studies where the boundary inclination has been investigated in addition to misorientation, as in the work of Pan et al., some very interesting things have been discovered [9]. Low angle boundaries and $\Sigma 3$ CSL boundaries seem to resist cracking regardless of boundary inclination while the remaining population of CSL boundaries in the study resisted cracking only when the correct boundary inclination and restrictive definition of CSL boundaries by Palumbo and Aust [5] were satisfied [9].

Very recently Rohrer et al. published a review on the distribution of internal interfaces in polycrystals [10]. The review is aimed at providing the current characteristics, methods and findings for investigations into the GBCD. In their study the energy of grain boundaries is discussed in terms of its relation to the GBCD, where boundary inclination plays a large role. The article also mentions that for specific materials no specific misorientations show preference for high coincidence boundaries

beyond the population of low angle and Σ3 boundaries. Instead, boundaries which should be considered special are those which are terminated by low-index planes, which can occur at any misorientation [10].

So, while it might be argued that the grain boundary inclination should or should not be included in the set of measured characteristics representing the GBCD, this paper does not attempt to prove this necessity. Rather, the work presented herein is aimed at describing a new and efficient technique through which one can obtain the grain boundary inclination parameters of the GBCD.

1.2 Current Measurement Techniques

To recover the GBCD including boundary inclination, a number of techniques exist, including but not limited to serial sectioning, x-ray methods, stereology and transmission electron microscopy (TEM) [10].

Serial sectioning, which is typically used to provide three-dimensional information such as connectivity or morphology [11-14], can also be used to recover the GBCD of a material [15]. Boundary inclinations are directly measured by this method and if the connectivity or morphology is not of interest the required number of section planes can be greatly reduced [15].

In contrast to serial sectioning, is the method of stereology where boundary inclination is never directly measured. Instead, stereology relies upon statistical methods and a large number of samples to recover the grain boundary character. The methodology requires a solution to inverse problems which can be quite complex and difficult to solve [16-18].

Also capable of recovering the GBCD are x-ray methods such as three-dimensional x-ray diffraction (3DXRD) and the differential aperture x-ray microscope (DAXM). These methods, which also directly measure boundary inclination, are nondestructive and can measure kinetic processes. However, these methods can be limited by their spatial resolution and require large radiation sources [19,20].

TEM, although capable of measuring the GBCD with a high degree of accuracy, requires considerable time to measure each boundary. As such, most studies are limited to a small number of boundaries and are thus insufficient to measure the GBCD for the entire material.

1.3 Aim and Approach

The new method presented in this article, called oblique double-sectioning (ODS), provides a new manner through which to recover the GBCD of a material. ODS might be best understood as a cross between stereology and serial sectioning, because this hybrid approach utilizes the advantages of serial sectioning's direct measurement of boundary inclination and stereology's statistical sampling of a material. This is accomplished by cutting a material into a set of smaller samples at oblique angles. Each sample in the set is then serially sectioned twice, to give two parallel layers of data from which the GBCD can be directly measured.

The solution to the method presented here is similar to the recovery of orientation distributions from incomplete pole figures as presented by H.-J. Bunge [21]. The ODS methodology has been presented previously by the authors but is presented here in an altered, more complete format with simulations to verify the

method [22]. To provide a reference for comparison, the simulations of the ODS methodology will also be compared with the L_A/S_V stereology of Adams [18].

2 The Grain Boundary Character Distribution

2.1 Definitions and Boundary Types

To define the GBCD in terms of a function we choose to use the following

$$S_V(\hat{n} \mid b)d\hat{n} = \frac{dS}{V} \tag{2-1}$$

where $\frac{dS}{V}$ is the grain boundary surface area per unit volume of material for boundaries of type *b* found in the vicinity $d\hat{n}$ of the direction $\hat{n}$. With this definition, the boundary type, *b*, can be adapted to describe those features at the boundary which are of greatest importance. The function $S_V(\hat{n} \mid b)$ will then allow the investigator to represent the habits of any specific grain boundary type.

When a complete crystallographic and geometric description of the GBCD is needed, the boundary type, *b*, must be defined by the orientation of the grains on either side of the boundary, *g* and *g*', as well as the inclination of the boundary itself, $\hat{n}$. Alternatively, the GBCD can be expressed solely in terms of the misorientation, Δg, and inclination, $\hat{n}$, of the grain boundary.

The crystallographic orientations, g, g' and Δg, of a boundary are typically represented in terms of three Euler angles, the domain of which is defined by the crystal symmetry of the material.

The boundary inclination $\hat{n}$ will be expressed in terms of spherical-polar angles ϕ and θ, where ϕ is the polar angle and θ is the azimuthal angle. The domain for the boundary inclination depends upon the reference frame selected for definition. Two commonly used reference frames in which boundary inclinations are defined are the crystal reference frame and the external sample reference frame. The selection of the reference frame depends upon why the boundaries are being investigated.

For boundary inclinations defined in the crystal frame, the material symmetry will determine the domain for the inclinations, while the domain for inclinations in the sample reference frame is typically limited to a sphere of directions, S^2. This domain can be reduced as well however, depending upon how the grain boundary type is chosen.

For the derivation provided here, all references to the boundary inclination will be given in the external sample reference frame. For further information on how the different crystal systems impact the domains of the parameters of $S_V(\Delta g, \hat{n})$, for $\hat{n}$ defined in the crystal frame, Rohrer et al. provides further information [10].

2.2 Representation

Although ODS is capable of recovering the GBCD for any number of different boundary types, only the grain boundary normal distribution, $S_V(\hat{n})$, of the GBCD

will be used in the derivation for clarity. The adaptation of ODS to recover the GBCD of other boundary types will be discussed later.

When written in terms of a Fourier series, the grain boundary normal distribution takes the form

$$S_V(\hat{n}) = \sum_{l=0}^{\infty} \sum_{m=-l}^{+l} S_l^m k_l^m(\hat{n}), \tag{2-2}$$

where $k_l^m(\hat{n})$ are the surface spherical harmonic basis functions as described by Bunge [21]. The ability of the Fourier series to resolve individual features of $S_V(\hat{n})$ is a function of the truncation order of the series. The full width at half the maximum value (*FWHM*) of a peak expressed by this Fourier series is defined as

$$FWHM = \frac{\pi}{L} \tag{2-3}$$

where L is the truncation order of the Fourier series. This allows one to determine individual peaks with a resolution of half the FWHM. In this article, the truncation order for all the Fourier Series was set at 22. The resolution for this truncation order would be ~ ± 0.07 rad or $\pm 4^\circ$.

2.3 Boundary Normal Symmetry

When the GBCD is expressed only in terms of the boundary inclination, $S_V(\hat{n})$, the domain of $\hat{n}$ is reduced from a sphere, S^2, to a hemisphere, RP^2. This results from the loss of sidedness, since a boundary with inclination $\hat{n}$ can no longer distinguish itself from a boundary with inclination $-\hat{n}$. From this, the grain boundary normal distribution obtains the following characteristic

$$S_V(\hat{n}) = S_V(-\hat{n}), \tag{2-4}$$

forcing $S_V(\hat{n})$ to become an even function. To account for this, the basis functions, $k_l^m(\hat{n})$, which are even functions only when the index l is even, force all the S_l^m coefficients with odd l indices to be zero. The resulting grain boundary normal distribution is given as

$$S_V(\hat{n}) = \sum_{l=0}^{L/2} \sum_{m=-2l}^{+2l} S_{2l}^m k_{2l}^m(\hat{n}) \tag{2-5}$$

where the truncation order of the series, L, must always be even.

3 Oblique Double-Sectioning

3.1 Framework

The ODS framework allows for the GBCD of the material to be obtained through direct measurement of the grain boundary parameters by sampling a set of section-cuts in the material. To obtain optimal statistical sampling, each sample in the set should be cut such that the normal of that sample be at an oblique angle to the rest of the samples in the set.

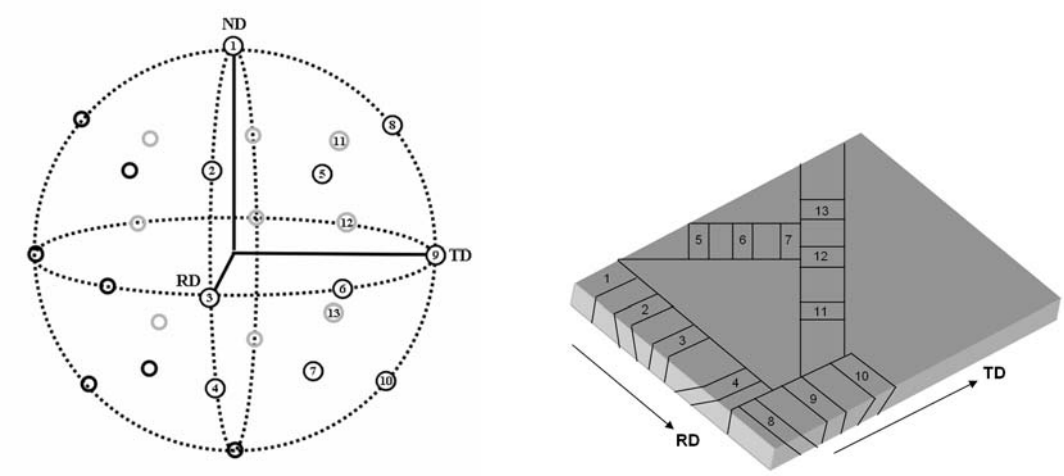

(a) **(b)**

Figure 3-1 (a) Sphere of directions representing the normal distribution for 13 oblique section-cuts along with their inverses. For clarity, points on the front half of the sphere are shown in black while points on the back half are shown in gray. (b) Representation of possible cutting scheme from single specimen. Numbered section-cuts correspond to the normal directions shown in (a).

While it can be conceived that ODS might be performed with as few as three orthogonal section-cuts, Figure 3-1 (a) shows the normals for a cutting scheme where 13 oblique section-cuts are employed. Figure 3-1 (b) shows how one could cut all 13 section-cuts from a single material.

Much of the following discussion concerning the acquisition of the measured GBCD from the material is based upon the methods of serial sectioning, and Saylor et al. provide an in-depth discussion of how one might perform this experimental data acquisition [15].

Each sample must be prepared such that the grain boundaries can be measured from the surface. The representative boundaries can be obtained from orientation imaging microscopy (OIM) maps or by etching the sample surface and using secondary electron imaging to recover the boundaries. If etching is used and the crystallography is of interest, OIM data will still be required for this purpose. A second layer, parallel to the first, must also be analyzed for the corresponding grain boundaries.

For the alignment of the parallel section-cuts fiducial marks (e.g. microhardness indents) or specific features of the microstructure (e.g. twin boundaries, triple junctions) which can be tracked through subsequent serial sections can be used to provide the necessary reference for the alignment [10]. Morawiec et al. also present a way in which an Affine transformation can be applied to statistical features to correct distortion that might have occurred during data acquisition [23].

After each double-section has been aligned, the measured boundaries must be extracted from the grain boundary measurements on the two parallel sections. Saylor

et al. describes a meshing algorithm that uses the measured boundaries to create a mesh of triangular surfaces representing the boundaries [15].

The measured GBCD can then be extracted from the grain boundary mesh by calculating the surface normal and surface area of each facet of the mesh. Then using the known volume of material that was removed between the double-sections the observed $S_V(\hat{n})$ can be obtained for that specific section-cut. If the same process is repeated on each of the oblique section-cuts one can obtain the required data needed to recover the overall GBCD for the material.

3.2 Mathematical Solution

The GBCD for the material is found by solving a least-squares best fit between the recovered data and the Fourier representation of $S_V(\hat{n})$. This choice of solutions helps to overcome the effect of incompletely measuring boundary inclinations through serial sectioning.

When serially sectioning a material, the boundaries of small grains have the potential to go unmeasured on both grain boundaries. Thus, the measure of incompleteness is a function of the depth removed between double-sections, *d*, and the average grain size of the material, $\langle GS \rangle$.

To defined this measure of incompleteness, we first recognize that the domain for boundaries lying in the hemisphere, RP^2, is given by $0 \le \phi \le \pi/2$, $0 \le \theta < 2\pi$. The

limit for the polar angle ϕ is reduced to $\phi_a \le \phi \le \pi/2$ where

$$\phi_a \approx \frac{d}{\langle GS \rangle}. \tag{3-1}$$

This artifact of error is present in all serial sectioning studies but typical ratios of ϕ_a are recommended to be small causing this error to be negligible.

ODS does have an advantage over serial sectioning studies when this error is concerned because the whole set of section-cuts allows several section-cuts to measure a boundary with normal $\hat{n}$ that might go unmeasured on one single section-cut. In fact, the distribution of oblique section-cut normals is designed with this overlap of measurements in mind, allowing one to ensure that no boundary type goes unmeasured. The hole in any one section-cut will be covered up by a number of other section-cuts.

To enumerate each individual set of double-sections we will use the index *c*. Measurements of the GBCD in the cth section-cut will be defined in the specified local orthonormal reference frame $\left\{ {}^{(c)}\hat{e}_i \right\}$ which is related to the external reference frame by g^c. For clarity, boundaries measured in the local reference frame will be denoted as $\hat{n}'$ or in spherical-polar angles ϕ', θ'. The observed GBCD of the cth section-cut can then be given as ${}^{c}S_V(\phi', \theta')_{obs.}$.

The goal here is to find the overall distribution of $S_V(\hat{n})$ defined in the external reference frame. But to begin we must first define the error between the measured and calculated distributions of ${}^{c}S_V(\hat{n}')$ defined in the local reference frame. This is given as

$$\int_0^{2\pi}\int_{\phi'_a}^{\pi/2}\left[{}^cS_V(\phi',\theta')_{obs.}-{}^cS_V(\phi',\theta')_{cal.}\right]^2\sin\phi' d\phi' d\theta' , \tag{3-2}$$

where ${}^cS_V(\phi',\theta')_{cal.}$ will be written in terms of a Fourier series. It can be shown that the coefficients, ${}^cS_{2l}^{\mu}$, for ${}^cS_V(\hat{n}')$, given in the local reference frame, are related to the coefficients, S_{2l}^m, for $S_V(\hat{n})$ in the external reference frame by

$${}^cS_{2l}^{\mu} = \sum_{m=-2l}^{+2l} S_{2l}^m T_{2l}^{\mu m}({}^cg) . \tag{3-3}$$

The $T_{2l}^{\mu m}({}^cg)$ functions given in equation 3-3 represent the generalized spherical harmonic functions as described by Bunge [21]. If the relationship in equation 3-3 is substituted into the Fourier series for ${}^cS_V(\phi',\theta')_{cal.}$ in equation 3-2 we obtain

$$\iint_B\left[{}^cS_V(\hat{n}')_{obs.}-\sum_{l=0}^{\infty}\sum_{m=-2l}^{+2l} S_{2l}^m\ {}^c\xi_{2l}^m(\hat{n}')\right]^2 d\hat{n}' . \tag{3-4}$$

Some reductions in variables have been introduced into equation 3-4 to simplify the notation and are defined as

$$B=\left\{\hat{n}'\equiv(\phi',\theta')\,|\,\phi'_a\le\phi'\le\pi/2, 0\le\theta'<2\pi\right\}, \tag{3-5}$$

$$d\hat{n}' = \sin\phi' d\phi' d\theta' \tag{3-6}$$

and

$${}^c\xi_{2l}^m(\hat{n}') = \sum_{\mu=-2l}^{+2l} T_{2l}^{\mu m}({}^cg)k_{2l}^{\mu}(\hat{n}') . \tag{3-7}$$

The coefficients for the overall GBCD can now be found by minimizing the error over all the observed section-cuts, N_C,

$$\sum_{c=1}^{N_c}\iint_B\left[{}^cS_V(\hat{n}')_{obs.}-\sum_{l=0}^{\infty}\sum_{m=-2l}^{+2l}S_{2l}^m\ {}^c\xi_{2l}^m(\hat{n}')\right]^2 d\hat{n}'=\min. \tag{3-8}$$

To solve for the S_{2l}^m coefficients, equation 3-8 is differentiated with respect to $S_{2l'}^{m'}$ to obtain

$$2\sum_{c=1}^{N_c}\iint_B\left[{}^cS_V(\hat{n}')_{obs.}-\sum_{l=0}^{L}\sum_{m=-2l}^{+2l}S_{2l}^m\,{}^c\xi_{2l}^m(\hat{n}')\right]{}^c\xi_{2l'}^{m'}(\hat{n}')d\hat{n}'=0. \tag{3-9}$$

From this the S_{2l}^m coefficients can be chosen from the set of equations with a minimum error in the solution. Equation 3-9 can be rearranged and simplified to be

$$\sum_{l=0}^{L}\sum_{m=-2l}^{+2l}S_{2l}^m\zeta_{2l2l'}^{mm'}=\alpha_{2l'}^{m'} \tag{3-10}$$

in terms of the reduced variables

$$\zeta_{2l2l'}^{mm'}=\sum_{c=1}^{N_c}\iint_B{}^c\xi_{2l'}^{m'}(\hat{n}')\,{}^c\xi_{2l}^m(\hat{n}')d\hat{n}' \tag{3-11}$$

and

$$\alpha_{2l'}^{m'}=\sum_{c=1}^{N_c}\iint_B{}^cS_V(\hat{n}')_{obs.}\,{}^c\xi_{2l'}^{m'}(\hat{n}')d\hat{n}'. \tag{3-12}$$

From inspection it can be seen that equation 3-10 represents an inhomogeneous set of equations where the desired coefficients, S_{2l}^m, can be determined from an equal number of equations and unknowns. This system of equations can be solved using standard numerical techniques to give the S_{2l}^m coefficients for the grain boundary normal distribution of the material.

Thus it can be seen that through the ODS methodology $S_V(\hat{n})$ can be recovered, although it is more likely though that one would rather recover the GBCD

for any set of boundaries of type *b*. To accommodate this, ODS simply requires that instead of providing all the measured boundary normals as input, only the boundaries of type *b* be used as the measured data. Then when ODS exports the grain boundary normal distribution $S_V(\hat{n})$, this distribution is representative for the boundaries of type *b* giving $S_V(\hat{n} \mid b)$.

3.3 Numerical Technique

In solving the ODS methodology, the calculation of the $\zeta_{2l2l'}^{mm'}$ coefficients represents the bulk of the computational cost. This large time cost comes from the long summations that are associated with the spherical harmonic basis functions. To reduce this computational time the following relationship was invoked

$$ {}^{c}\xi_{2l}^{m}(\hat{n}') = \sum_{\mu=-2l}^{+2l} T_{2l}^{\mu m}({}^{c}g) k_{2l}^{\mu}(\hat{n}') \equiv k_{2l}^{m}(\hat{n}), \tag{3-13} $$

In other words, when calculating ${}^{c}\xi_{2l}^{m}(\hat{n}')$, one doesn't have to perform the long summations associated with ${}^{c}\xi_{2l}^{m}(\hat{n}')$. Instead, the boundary normal $\hat{n}'$ can simply be rotated from the local reference frame into the external reference frame and the surface spherical harmonic basis functions need only be called once with the rotated normal $\hat{n}$.

In addition, the following relationship is true

$$ \zeta_{2l2l'}^{mm'} = \zeta_{2l'2l}^{m'm}, \tag{3-14} $$

which means that once $\zeta_{2l2l'}^{mm'}$ has been computed, $\zeta_{2l'2l}^{m'm}$ has also been worked out, reducing the number of calculations necessary to calculate all the $\zeta_{2l2l'}^{mm'}$ variables.

When all the $\zeta_{2l2l'}^{mm'}$ coefficients have been calculated, they can be tabulated for easy reference when solving the ODS methodology.

These two properties substantially increased the speed of the calculation of the $\zeta_{2l2l'}^{mm'}$ coefficients which need only be calculated once and then tabulated for use in the remainder of the ODS calculations.

Another technique can be employed to increase both the accuracy and speed of the calculation of $\alpha_{2l'}^{m'}$. This is accomplished by discretizing the reduced RP^2, or area defined by B, into I discrete elements, and employing the Dirac function, $\delta(\hat{n}' - \hat{n}_i')$, with the following property

$$\iint_B \delta(\hat{n}' - \hat{n}_i') d\hat{n}' = 1. \tag{3-15}$$

Using the Dirac function, ${}^cS_V(\hat{n}')$ becomes

$${}^cS_V(\hat{n}') = \sum_{i=1}^{I} {}^cS_V^i \delta(\hat{n}' - \hat{n}_i') \tag{3-16}$$

where ${}^cS_V^i$ represents the surface area per unit volume of boundaries in the direction of $\hat{n}_i'$ on the c^{th} section-cut. By inserting ${}^cS_V(\hat{n}')$ as defined by equation 3-16 into equation 3-12 we obtain

$$\alpha_{2l'}^{m'} = \sum_{c=1}^{N_c} \iint_B \sum_{i=1}^{I} {}^cS_V^i \delta(\hat{n}' - \hat{n}_i') \; {}^c\xi_{2l'}^{m'}(\hat{n}') d\hat{n}'. \tag{3-17}$$

This can then be reduced to

$$\alpha_{2l'}^{m'} = \sum_{c=1}^{N_c} \sum_{i=1}^{I} {}^cS_V^i \, {}^c\xi_{2l'}^{m'}(\hat{n}_i') \tag{3-18}$$

by using the definition of the Dirac function. This reduction substantially increases the speed and accuracy of the calculations.

One final way to increase the speed of the calculation of the $\alpha_{2l'}^{m'}$ coefficients is to substitute the definition of ${}^{c}\xi_{2l}^{m}(\hat{n}')$ as defined by equation 3-13 into equation 3-18; similar to that performed in the calculation of the $\zeta_{2l2l'}^{mm'}$ coefficients.

4 Validation of ODS

4.1 Simulation

To validate the ODS methodology, computer simulations were used. The simulations were created by filling a simulated volume with a large number of discs, each of which was given an associated area and normal. An illustration of the simulation is given in Figure 4-1. The distribution of normals was varied throughout a number of simulations, although only the results for a single distribution of normals will be presented here.

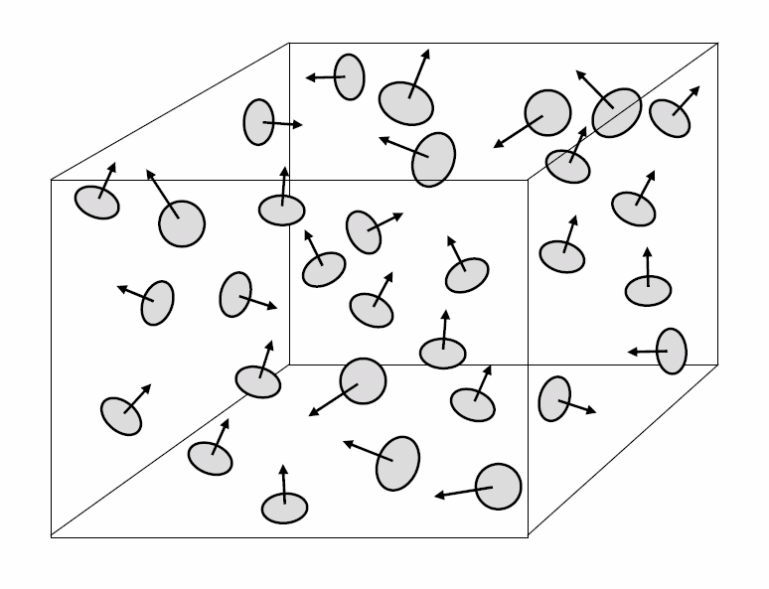

Figure 4-1 Illustration of disc simulation within volume.

The simulated volume was measured for the distribution of section-cuts shown in Figure 3-1 . The simulated volume was sectioned with several oblique double-sections and only the normal and area of the discs measured between the two discs were used in the calculations.

The solution to the ODS simulation was carried out for different combinations of the section-cuts to simulate measurements as if only a certain number of section-cuts were present. The scheme by which the solution to the simulations was solved is given in Table 4-1 where the number referencing specific section-cuts corresponds to the number of the section-cut shown in Figure 3-1 .

Table 4-1 Cutting schemes for ODS simulations

Number of Section-Cuts	*Section-Cuts used from Figure 3-1*
1	1
2	1,3
3	1,3,9
5	1,5,7,11,13
7	1,3,5,7,9,11,13
9	1,3,5-7,9,11-13
11	1-5,7-11,13
13	1-13

While it was possible to accurately measure the inclination and surface area of each of the discs, the simulation was adapted to reflect the imperfect measurements of experimental recovery. The errors of the measurements were consistent with those of

current measurement techniques where the polar angle of the boundary inclination can be recovered with less accuracy than the azimuthal angle.

The measured simulations were compared against the true distribution whose coefficients can be determined by

$$^{T}S_{2l}^{m} = 2\sum_{j=1}^{J} S_V^j k_{2l}^{*m}(\hat{n}_j) \qquad (4\text{-}1)$$

where the sum over *j* represents the sum over all the discs in the volume. The * on the basis function in equation 4-1 denotes the complex conjugate and the factor of 2 comes from the fact that $S_V(\hat{n}) = S_V(-\hat{n})$, so the inverse direction, $-\hat{n}$, must also be accounted for.

The distribution for the simulations can be seen in Figure 4-2 where (a) represents the true solution for $S_V(\hat{n})$. The remaining plots in Figure 4-2, (b)-(i), represent the recovered $S_V(\hat{n})$ based upon a specific number of section-cuts sampled, as described by the label below each plot. In the ODS methodology, the variable ϕ_a, representing the incomplete measuring of the data, was given the value of 0.1 while truncation order for all the Fourier series was set at *L*=22.

As can be seen in the plots of Figure 4-2, there are 3 specific peaks which were placed in the simulation, but these only represent 50% of the boundaries. The remaining 50% of the boundaries were randomly placed around the hemisphere, to see how well the method worked with noise present.

From a visual analysis of Figure 4-2, it appears that for any distribution where at least 3 section-cuts were measured, ODS is able to recover a distribution similar to the true solution.

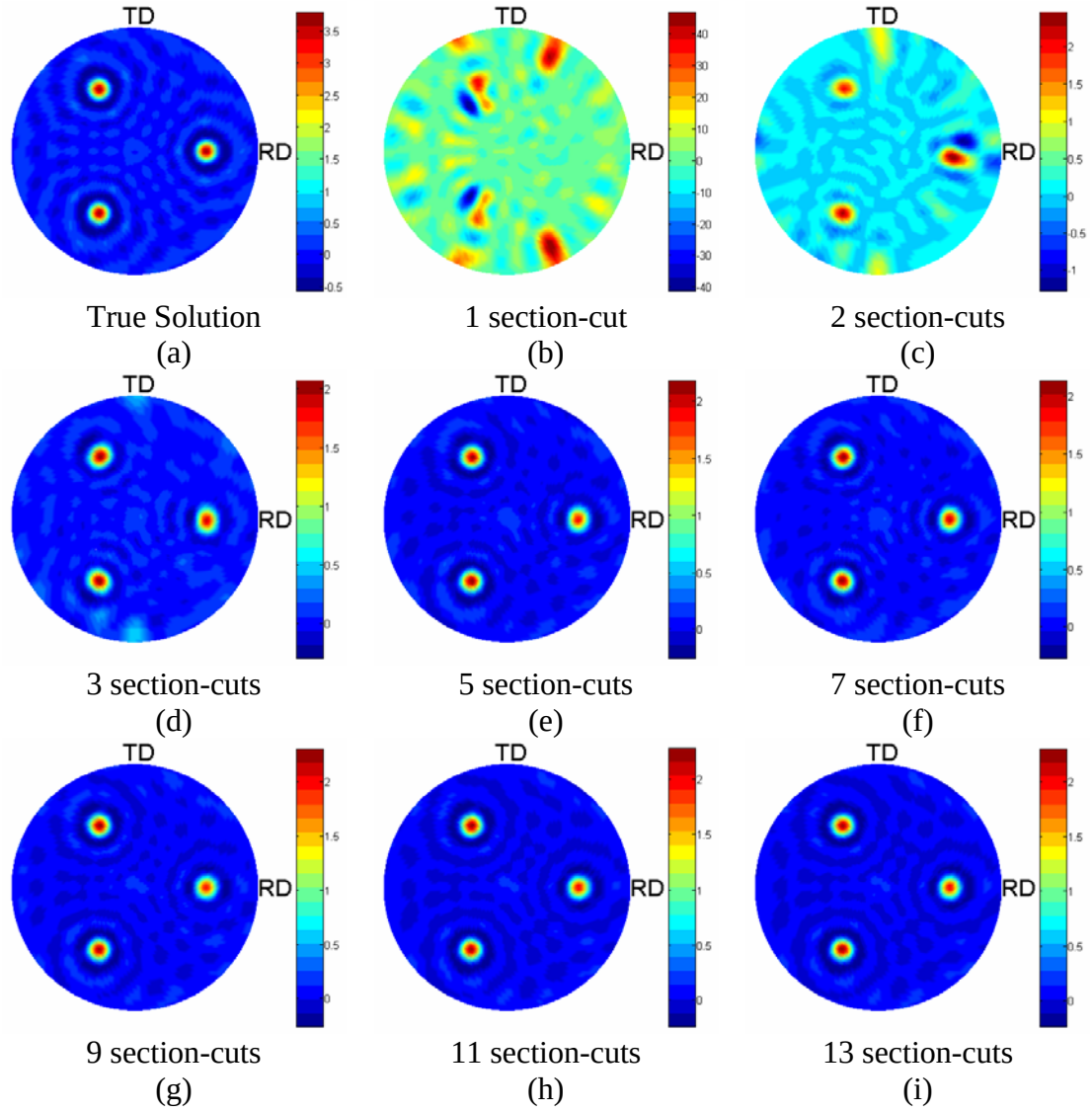

Figure 4-2 True and measured $S_V(\hat{n})$ plots from simulations of the cutting scheme given in Table 4-1.

The error associated with the solutions can be calculated as a measure of the distance between the true grain boundary normal distribution, ${}^{T}S_V(\hat{n})$, and the measured grain boundary normal distribution , ${}^{M}S_V(\hat{n})$, as

$$\Xi = \oiint_{S^2} \left({}^{T}S_V(\hat{n}) - {}^{M}S_V(\hat{n}) \right)^2 d\hat{n} . \qquad (4\text{-}2)$$

When Ξ is expressed as a Fourier series, the error can be reduced to

$$\Xi = \sum_{l=0}^{L/2} \Xi(2l) \tag{4-3}$$

where

$$\Xi(2l) = \sum_{m=-2l}^{+2l} \left[{}^{T}S_{2l}^{m} - {}^{M}S_{2l}^{m} \right]^2 . \tag{4-4}$$

The plot of $\Xi(2l)$ for the simulations is shown in Figure 4-3. From Figure 4-2 and Figure 4-3 it can be seen that one and two section-cuts are insufficient to recover the true grain boundary normal distribution that exists in the volume by ODS. In contrast it can be seen that anywhere from three to thirteen section-cuts recovers approximately the same distributions with very little error.

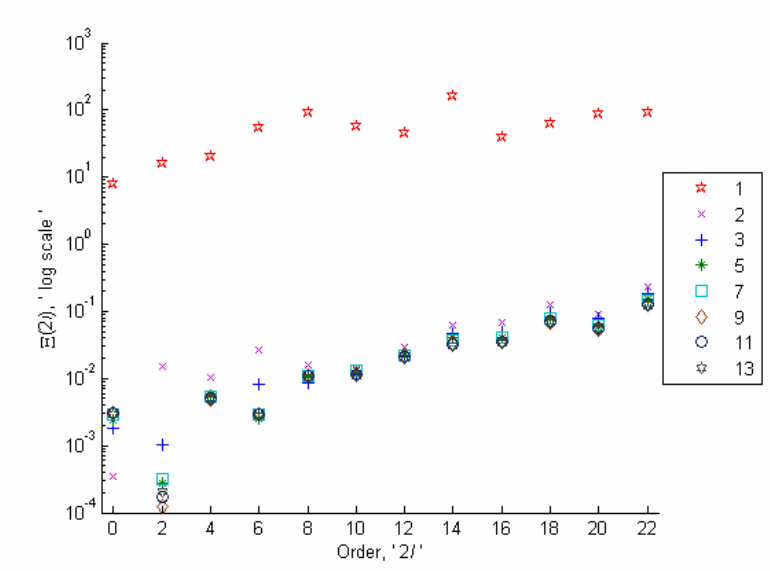

Figure 4-3 Error plot, $\Xi(2l)$, for a given number of section-cuts as described in Table 4-1.

4.2 Zeta Calculations

During the derivation of the ODS methodology it became apparent that although $\zeta_{2l2l'}^{mm'}$ coefficients could be tabulated, they were going to have to be calculated using numerical integration. In our calculations, a recursive integration routine was used to find the solution within a specific tolerance. Although a really low tolerance would have been preferential, a decrease in the tolerance requires an exponential increase in calculation time.

To discover a minimum tolerance required, the ODS methodology was solved repeatedly for three section-cuts for different integration tolerances on the $\zeta_{2l2l'}^{mm'}$ coefficients as well as to different orders of truncation. When each boundary was measured in the simulation, the exact angles and area were used to limit the effect of any additional error to the $\zeta_{2l2l'}^{mm'}$ coefficients.

These results were then used to calculate the error function Ξ, as defined in equation 4-3. It is important to note that this error function differs from the previously mentioned error function $\Xi(2l)$ defined in equation 4-4. The error function in equation 4-3 gives the total error of the distribution and not just the error for specific coefficients. The Ξ error function is plotted in Figure 4-4, but also differs from the plots of $\Xi(2l)$ because each marker in the graph represents the total error for the ODS methodology solved to the truncation order $2l$.

Interpreting the data in Figure 4-4 takes some care and we must recall that the solution to ODS requires the $\zeta_{2l2l'}^{mm'}$ coefficients to be inverted to solve for the unknown S_{2l}^{m} coefficients representing the grain boundary normal distribution. Since matrix

inversion becomes impossible for ill-conditioned matrices care must be taken to ensure that the $\zeta_{2l2l'}^{mm'}$ coefficients do not represent an ill-conditioned matrix. To do this one can examine the condition number of a matrix, where a matrix condition number near 1 indicates a well-conditioned matrix, and the higher the condition number gets, the more difficult it will be to invert. Ill-conditioned matrices which have an infinite condition number are singular and therefore have no matrix inverse [24].

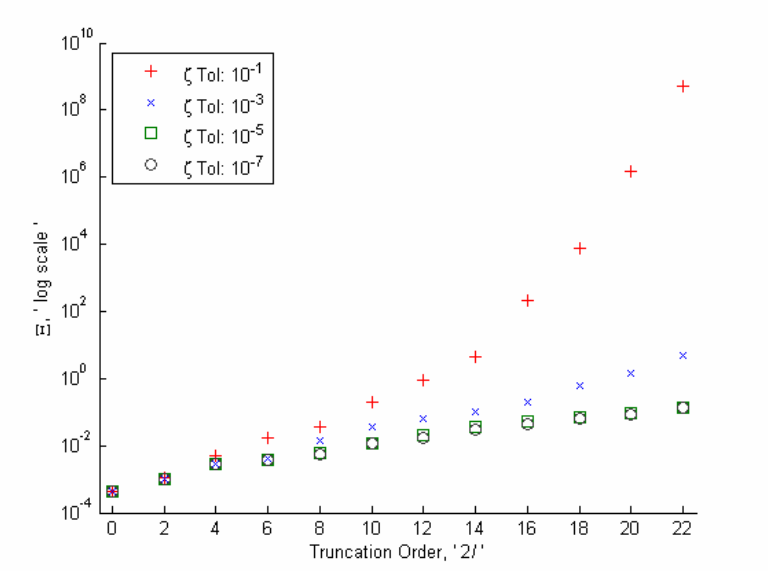

Figure 4-4 Error plot, Ξ, of ODS methodology for the $\zeta_{2l2l'}^{mm'}$ coefficients integrated to different tolerances.

Consider the solution to the ODS methodology using the $\zeta_{2l2l'}^{mm'}$ coefficients solved to the tolerance 10^{-1}. It is understood that as the truncation order of the Fourier series is increased that the number of unknowns increases exponentially. So as truncation order of the series increases, but the nature of the matrix remains the same, the more difficult this matrix will be to invert. This is illustrated by the increasing errors in the plot as the truncation order is increased. If we examine the markers for

the differing tolerances on the $\zeta_{2l2l'}^{mm'}$ coefficients we can see that even as the truncation order increases, the total error Ξ increases at a much slower rate for lower tolerances. In examining the condition numbers of all the matrices being inverted, it was noticed that they increased in the same trends as did the error in Figure 4-4.

From this one can see that if one desires to resolve specific features in the distribution of $S_{V'}(\hat{n})$, the truncation order of the Fourier series must be increased. This in turn requires that the accuracy of the $\zeta_{2l2l'}^{mm'}$ coefficients be increased for proper inversion and solution to the equations of ODS, although it can be seen that a tolerance of 10^{-5} will have approximately as little error as 10^{-7}. For this reason, it was determined that the tolerance of 10^{-5} was sufficient to solve the ODS simulations.

In addition, the inversion of the $\zeta_{2l2l'}^{mm'}$ coefficients can be improved by an increased number of measured section-cuts, because the condition of the matrix improves with each additional section-cut. This will not only improve the inversion process but also increase the accuracy of the method by having an even better statistical sampling of the microstructure. This also helps to explain the error of the simulations when solved with 1 and 2 section-cuts as shown in Figure 4-2 and Figure 4-3. The condition number of both of these matrices was extremely large meaning that the inverted matrix was most likely in too poor of a state to give an accurate solution.

5 Stereological Comparison

5.1 Review of Stereology

For further validation and comparison, the grain boundary normal distribution recovered by ODS was compared to that recovered by the L_A/S_V stereology. As mentioned previously, the L_A/S_V stereology is a method which recovers $S_V(\hat{n})$ by statistically sampling grain boundaries from oblique section-planes, as described by Adams and Field [18]. Since a complete understanding of this stereology would be too much to present here, we provide a brief description of a few key equations required to solve for the grain boundary normal distribution, $S_V(\hat{n})$.

For boundaries observed from a single section-cut, a convenient function for representation is $L_A(\omega \mid b)$ or line length per unit area of boundary type *b*. The angle ω only represents the azimuthal angle for the boundary normal $\hat{n}$; meaning that the inclination of the boundary goes undefined. But when enough boundaries are sampled from a set of oblique section-cuts, the statistics of the sampling method provide the a measure for the boundary inclination, giving $S_V(\hat{n})$. Thus, if one can accurately measure $L_A(\omega \mid b)$ one can recover the GBCD, $S_V(\hat{n} \mid b)$.

In the brief overview of the L_A/S_V stereology we start with the $L_A(\omega)$ function. For boundaries measured on the jth section-plane we choose to represent $L_A(\omega)$ as a Fourier series

$$ {}^{j}L_A(\omega) = \sum_{t=-\infty}^{\infty} L_t^j e^{it\omega} . \tag{5-1} $$

In their derivation, Adams and Field show that the L_t^j coefficients are related to the S_l^m coefficients for the grain boundary normal distribution in equation 2-2 by

$$ L_t^j = \frac{1}{\sqrt{2\pi}} \sum_{l=|t|}^{L} \sum_{m=-l}^{l} S_l^m T_l^{mt} ({}^{j}Q) I_l^t . \tag{5-2} $$

Equation 5-2 represents an over-determined set of equations (the S_l^m coefficients are unknown), which can be solved by traditional mathematical methods. Adams and Field show that to accurately solve $S_V(\hat{n})$ to the truncation order L, L+1 section-planes are required. This in turns affects the ability of the function $S_V(\hat{n})$ to resolve specific peaks in the distribution because as was shown earlier in equation 2-3, the *FWHM* of peaks in the distribution are a function of the truncation order L.

5.2 Comparison of ODS and L_A/S_V Stereology

To compare ODS and the L_A/S_V stereology the results from simulations with discs in a volume were employed. In measuring the discs from each double section-cut, only those discs which were measured by both layers of the section-cut were used for the ODS data, while any disc that crossed the bottom of the two layers of each section-cut was used for the stereological data. Again, the measurement of each disc

was adjusted to approximate the real errors associated with experimental measurements.

The grain boundary normal distribution was then solved by each of the methods and is presented in Figure 5-1. The stereological equations previously presented were adapted to recover the even l coefficients, or S_{2l}^{m}, similar to the ODS methodology. The error plots, $\Xi(2l)$ and Ξ, for the distributions recovered by both methods are shown in Figure 5-2.

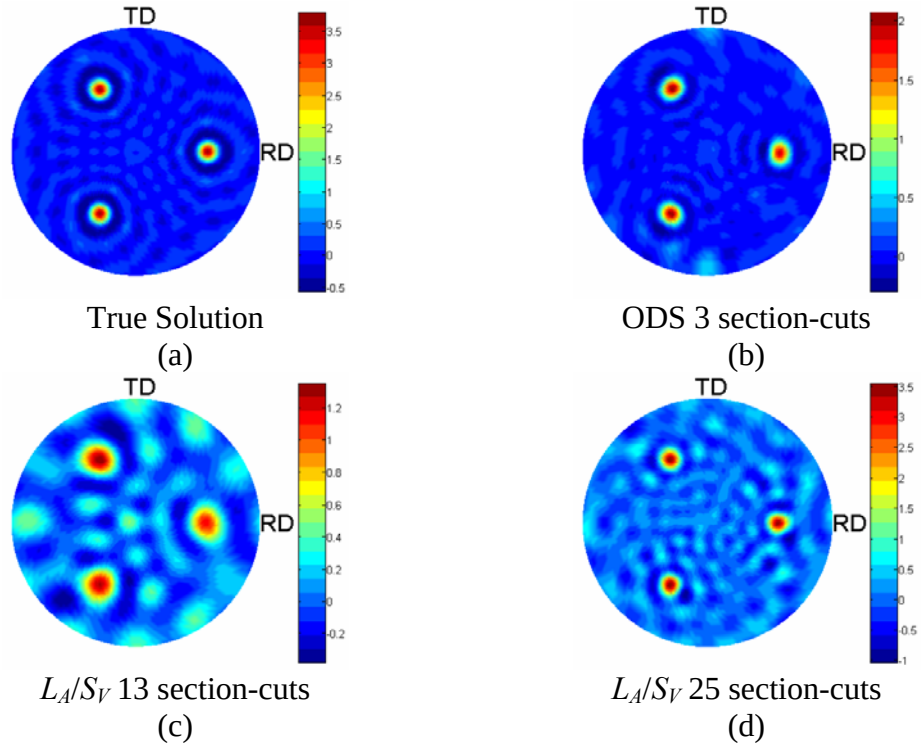

True Solution
(a)

ODS 3 section-cuts
(b)

L_A/S_V 13 section-cuts
(c)

L_A/S_V 25 section-cuts
(d)

Figure 5-1 True and measured $S_V(\hat{n})$ plots from simulations for comparison of ODS and the L_A/S_V stereology.

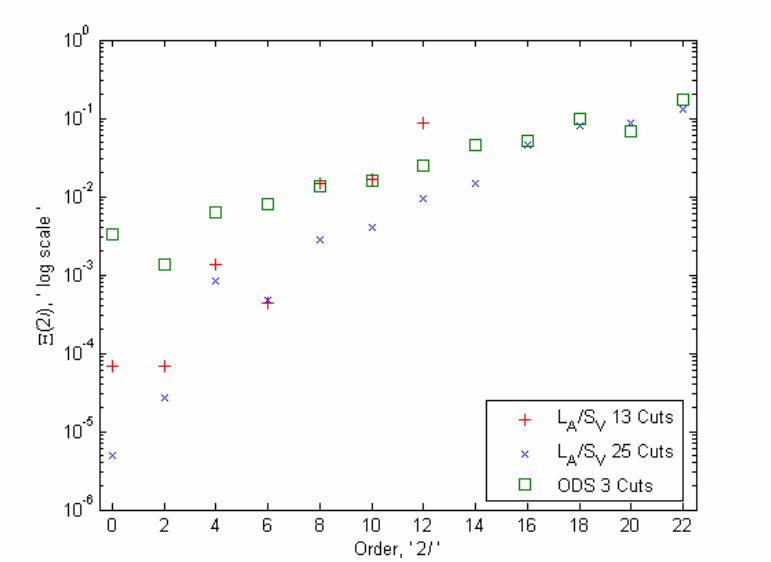

(a)

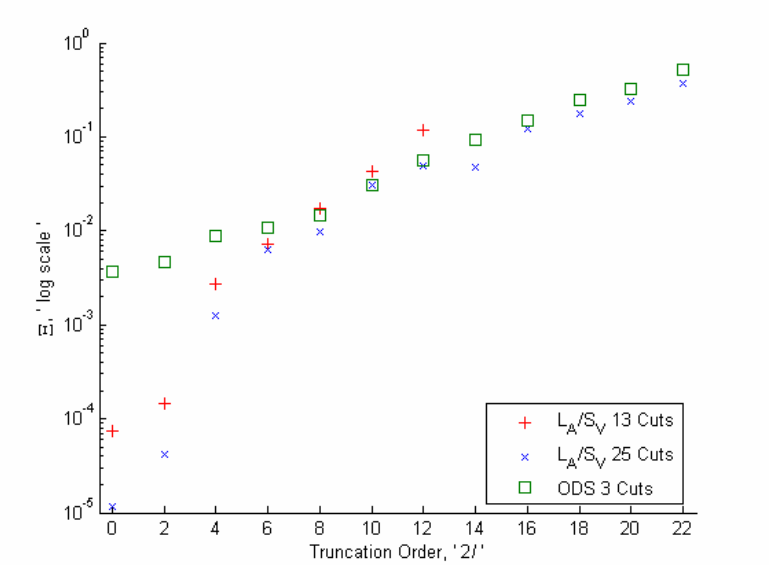

(b)

Figure 5-2 Error plots for comparison of ODS and the L_A/S_V stereology where (a) is the $\Xi(2l)$ error plot and (b) is the Ξ total error plot.

From Figure 5-1 and Figure 5-2 it is clear that both ODS and the L_A/S_V stereology are capable of recovering the simulated distributions. It is noted that the stereological functions do have a little more variation in their distributions than the true distribution as can be seen in Figure 5-1. This is most likely due to the noise, or 50% random boundaries. Even when 25 simulated cuts were used with the stereology,

the distribution still fails to appear exactly as the true distribution. To explain this we must look at the error plot in Figure 5-2(a). Here we see that the stereologically recovered distributions actually perform better than the ODS in the lower order coefficients, although an error of ~10^{-3} is not large.

The higher order coefficients of the series are responsible for making the distributions resolve specific features and as can be seen from the distribution and error plots, the stereology struggles with these higher order coefficients. From the Ξ error plot in Figure 5-2(b) we see that for an increasing truncation order the total error is approximately the same for the 3 cuts of ODS and 25 cuts of the stereology.

It is also noted that with the 13 section-cuts of the L_A/S_V stereology, the truncation order is limited to 12, forcing the distribution to have broad peaks. This shorter truncation order also makes error calculations beyond 12^{th} order impossible. ODS has the ability to resolve these higher order coefficients even when data from only a few section-cuts is available, because the truncation order of ODS is not limited by the number of section-cuts available.

It is speculated that the reason the error for the lower order coefficients of ODS is greater than the error for the L_A/S_V stereology is on account of the incomplete measuring of ODS. As was mentioned previously, boundaries with normals nearly parallel to the normal of the section-cut will have the tendency to go unmeasured.

So while ODS measures all the habits of the boundaries with as few as 3 cuts, a number of boundaries are missed in each section-cut. Thus the lower order coefficients, which are responsible for estimating the magnitude of the distribution of measured boundaries, will have greater error when compared with the stereology. But

again it is important to note that while the error of the lower order coefficients is greater than that for the stereology, the error is still only on the order of 10^{-3} to 10^{-2}.

While ODS may not perform any better than the L_A/S_V stereology, ODS was able to recover the same distribution as the stereology with 3 double-sections instead of the 25 cuts required by stereology.

6 Discussion and Conclusions

In this article it has been shown that the new method called oblique double-sectioning (ODS) is capable of recovering the boundary inclination parameters of the grain boundary character distribution (GBCD). Through the derivation of the methodology and the simulations of ODS we have shown that:

- The ODS methodology uses serial sectioning's direct measurement of boundary inclination parameters while providing a statistical sampling of the microstructures similar to that obtainable through stereology.
- The solution framework provides a robust solution of the grain boundary normal distribution of a material when the measured data is representative of that found in the material.
- From simulations we can see that while 1 and 2 section-cuts are insufficient for an accurate representation, 3 section-cuts provide a solution nearly identical to that obtained from 5 to 13 section-cuts. This indicates that 3 orthogonal double section-cuts should be sufficient to carry out the ODS methodology.
- The truncation order on the Fourier series representing the solution is independent of the number of section-cuts of available data.

- The solution to the ODS methodology requires the solution to an inverse problem and care must be taken to ensure a good degree of accuracy.

When the results of ODS simulations are compared with the L_A/S_V stereology of Adams we see that:

- The stereological recovery of the GBCD requires the number of section-cuts to be one greater than the truncation order of the series. In contrast, ODS does not require an exact number of section-cuts to achieve any specific truncation order.
- The stereological recovery of the GBCD is more accurate in recovering the lower order coefficients of the GBCD than ODS is, although the error for ODS is relatively small, 10^{-2}.
- As a result of the direct measurement of the boundary inclination parameters, ODS with as few as 3 section-cuts can resolve the specific habits of grain boundary planes as accurately as 25 section-cuts with stereology.

7 References

[1] Sutton, A. P. and Balluffi R.W., Interfaces in Crystalline Materials, Clarendon Press, Oxford, 1995.

[2] Kumar, M. and Schuh, C. A., Scripta Mater 2006;54:961.

[3] Watanabe, T., Tsurekawa, S., Zhao, X., and Zuo, L., Scripta Mater 2006;54:969.

[4] Schwartz, A. J., King, W. E., and Kumar, M., Scripta Mater 2006;54:963.

[5] Palumbo, G. and Aust, K. T., Acta Metall Mater 1990;38:2343.

[6] Palumbo, G., King, P. J., Aust, K. T., Erb, U., and Lichtenberger, P. C., Scripta Metall Mater 1991;25:1775.

[7] Crawford, D. C. and Was, G. S., Metall trans A 1992;23:1195.

[8] Lin, P., Palumbo, G., Erb, U., and Aust, K. T., Scripta Metall Mater 1995;33:1387.

[9] Pan, Y., Adams, B. L., Olson, T., and Panayotou, N., Acta Mater 1996;44:4685.

[10] Rohrer, G. S., Saylor, D. M., El Dasher, B., Adams, B. L., Rollett, A. D., and Wynblatt, P., Z Metallkd 2004;95:197.

[11] DeHoff, R. T., J Microscopy 1983;131:259.

[12] Rhines, F. N., Craig, K. R., and Rousse, D. A., Metall Trans A 1976;7A:1729.

[13] Kral, M. V. and Spanos, G., Acta Mater 1999;47:711.

[14] Zhang, C., Suzuki, A., Ishimaru, T., and Enomoto, M., Metall Mater Trans A 2004;35A:1927.

[15] Saylor, D. M., Morawiec, A., and Rohrer, G. S., Acta Mater 2003;51:3663.

[16] Hilliard J.E., T Metall Soc AIME 1962;224:1201.

[17] Adams, B. L., Metall Trans A 1986;17:2199.

[18] Adams, B. L. and Field, D. P., Metall Trans A 1992;23:2501.

[19] Poulsen, H. F., Appl Physics A-Mater 2002;74:S1673.

[20] Liu, W. J., Ice, G. E., Larson, B. C., Yang, W. G., Tischler, J. Z., and Budai, J. D., Metall Mater Trans A 2004;35A:1963.

[21] Bunge, H.-J., Texture Analysis in Materials Science, Cuvillier Verlag, Göttingen, 1993.

[22] Homer, E. R., Adams, B. L., and Fullwood, D. T., Scripta Mater 2006;54:1017.

[23] Morawiec, A. and Saylor, D. M., Proceedings ICOTOM 12, 1999 p.198.

[24] Kincaid, D. and Cheney, W., Numerical Analysis: Mathematics of Scientific Computing, 3rd ed., Brooks/Cole, Pacific Grove, 2002.